Proceedings of the ASME 2026 45th International
Conference on Ocean, Offshore and Arctic Engineering
OMAE2026
June 7-12, 2026, Tokyo, Japan

OMAE2026-181953

A CFD INVESTIGATION OF WAVE-CURRENT COUPLING EFFECTS ON THE DYNAMIC RESPONSE OF A TLP FOWT

Yisheng Yao
Computational Marine Hydrodynamic Lab (CMHL), School of Ocean and Civil Engineering, Shanghai Jiao Tong University, Shanghai, China

Maokun Ye
Computational Marine Hydrodynamic Lab (CMHL), School of Ocean and Civil Engineering, Shanghai Jiao Tong University, Shanghai, China

Shiyuan Zhang
Offshore Oil Engineering Co. Ltd Tianjin, China

Decheng Wan*
Computational Marine Hydrodynamic Lab (CMHL), School of Ocean and Civil Engineering, Shanghai Jiao Tong University, Shanghai, China

ABSTRACT

Tension Leg Platforms (TLPs) are characterized by a shallow draft, compact structural configuration, and favorable cost efficiency, making them a candidate concept for large-scale offshore wind deployment in deep and remote waters. By utilizing pretensioned tendons to balance excess buoyancy, TLP-based floating offshore wind turbines (FOWTs) exhibit high global stiffness, which elevates their natural frequencies in heave and pitch. As a result, these platforms are particularly sensitive to high-frequency hydrodynamic excitations. Although wave–current coupling has been observed in model tests and numerical simulations to amplify high-frequency heave motions in other floating platform types, the resulting motion responses in those systems generally remain moderate owing to their lower natural frequencies. In contrast, for TLP FOWTs, the influence of wave–current interaction on high-frequency dynamics remains underexplored, despite its potential significance. Conventional wave-current coupling analysis methods based on potential flow theory struggle to accurately simulate the actual effects of ocean currents and can only rely on the Morison element method for simplification, whereas the CFD method boasts inherent advantages in addressing wave-current coupling problems. To address this gap, this study employs high-fidelity Computational Fluid Dynamics (CFD) to investigate a TLP supporting the NREL 5 MW reference wind turbine, with particular emphasis on quantifying the effect of wave–current coupling on platform motion responses. The results demonstrate that, under combined wave–current conditions, the TLP FOWT experiences significant amplification in surge, heave and pitch motions. This enhanced motion response leads to a substantial increase in peak loads on the tendon mooring system, highlighting the critical need to account for wave–current interaction in the dynamic analysis and design of TLP-based offshore wind systems.

Keywords: Tension Leg Platform (TLP); Floating Offshore Wind Turbine (FOWT); Wave-Current Coupling; CFD

1. INTRODUCTION

Offshore wind platforms are primarily classified into three categories based on structural design features and application scenarios: Spar platforms, semi-submersible platforms, and Tension Leg Platforms (TLPs) [1]. Among these, traditional Spar platforms, featuring a simple structure, are better suited for nearshore shallow-water areas with relatively mild sea conditions. In contrast, semi-submersible platforms and TLPs boast superior hydrodynamic performance and can maintain excellent motion stability even in deep and far-reaching offshore regions. TLPs adopt a vertical tension mooring system, which drastically cuts down steel usage—this not only reduces platform manufacturing costs but also significantly lowers its self-weight. Meanwhile, the high stiffness of this mooring system minimizes the vertical movement of TLPs, endowing them with markedly better stability than semi-submersible platforms [2]. Additionally, the vertical arrangement of TLPs' mooring lines results in a much smaller mooring radius compared with semi-submersible platforms, thereby saving offshore space and facilitating the intensive layout of wind farms. In practical service conditions, TLPs are usually subjected to the combined action of wind, wave, and current loads. Although many scholars have carried out research on the motion responses of TLPs under wind and wave loads via methods like physical model tests or numerical simulations, most research teams use scaled-down models for basin experiments [3], which inevitably introduce scale conversion errors into the test results. In numerical simulations, full-scale model simulations can be directly conducted using software such as OpenFAST [4]. However, most of these numerical simulation tools are developed based on potential flow theory. Generally, ocean currents are modeled by calculating relative velocities, then computing current loads in the form of Morison elements [5], which are linearly superimposed with wave loads. Even though added damping is incorporated to simulate viscous effects, there is still a considerable gap between the simulation results and actual wave-current coupling effects. Some research teams have found that wave-current coupling can amplify high-frequency heave motions in certain types of platforms. For platforms with non-vertical mooring systems, this amplification effect is less significant. Nevertheless, TLPs have a relatively short natural heave period and are highly sensitive to high-frequency hydrodynamic excitations. Therefore, the impact of wave-current coupling on the heave motions of TLPs cannot be overlooked.

In this study, the in-house solver FOWT-ULAM-SJTU [6] solver is adopted, with the Tension Leg Platform (TLP) equipped with the National Renewable Energy Laboratory (NREL) 5 MW reference wind turbine as the research subject. The study aims to quantify the influence of wave-current coupling effects on platform motion responses and clarify the underlying mechanism of such influence through flow field analysis.

2. MATERIALS AND METHODS

Based on the open-source software OpenFOAM, this work conducts CFD numerical simulations using the team's self-developed integrated aero-hydro-mooring analysis solver FOWT-ULAM-SJTU. The aerodynamic module is solved by the actuator line model (ALM) [7]. The hydrodynamic calculation module is derived from the self-developed solver naoe-FOAM-SJTU, which enables the simulation of waves and ocean currents and solves the six-degree-of-freedom (6-DOF) motions of floating bodies. The mooring module solves the mooring lines based on the lumped mass method (LMM).

2.1 Governing Equations

In this work, the Navier-Stokes equations are adopted as the governing equations, which consist of two components: the continuity equation and the momentum equation. The incompressible flow assumption is incorporated into the self-developed solver, and the final form of the equations is given as follows:

$$\nabla \cdot \boldsymbol{U} = 0 \tag{1}$$

$$\frac{\partial \rho \boldsymbol{U}}{\partial t} + \nabla \cdot (\rho \boldsymbol{U} \mathrm{U}) = -\nabla p_{\mathrm{d}} - \boldsymbol{g} \cdot \boldsymbol{x} \nabla \rho + \nabla \cdot (\mu_{\mathrm{eff}} \cdot \nabla \boldsymbol{U}) \tag{2}$$

where $\boldsymbol{U}$ is the flow field velocity, ρ is the fluid density, p_{d} is the dynamic pressure, $\boldsymbol{g}$ is the gravitation acceleration, μ_{eff} is the dynamic viscosity.

2.2 Turbulence Model

This work adopts the Large Eddy Simulation (LES) approach for numerical calculations. The LES method employs spatial filtering to distinguish vortex structures of different scales in the flow field: large-scale vortices are directly resolved, while small-scale vortices are approximated using subgrid-scale models. The Smagorinsky model is adopted as the subgrid-scale (SGS) model, and the subgrid-scale stress is expressed as follows:

$$\tau_{\mathrm{ij}} = 2\nu_{\mathrm{SGS}} \overline{\tau_{\mathrm{ij}}} - \frac{1}{3} \tau_{\mathrm{kk}} \delta_{\mathrm{ij}} \tag{3}$$

where ν_{SGS} is the subgrid-scale viscosity and defined as follow：

$$\nu_{\mathrm{SGS}} = (C_{\mathrm{S}} \Delta)^2 \sqrt{2 \overline{S_{\mathrm{ij}}} \overline{S_{\mathrm{ij}}}} \tag{4}$$

where C_{S} is the Smagorinsky coefficient.

2.3 Numerical Wave And Current Generation

The numerical wave generation module and current generation method in the self-developed solver are implemented by specifying the fluid volume fraction and fluid velocity at the inlet boundary, and the specific methodologies have been elaborated and validated in our previous work.

The wave surface equation of regular waves is given as follows:

$$\eta = \frac{H}{2} \cos{(k\mathrm{x} - \omega \mathrm{t} + \varphi)} \tag{5}$$

where η is the wave surface elevation, H is the wave height, k is the wave number, x is the horizontal coordinate, ω is the angular frequency, t is the time, φ is the initial phase angle.

It is assumed that the current direction is consistent with the wave propagation direction; thus, the horizontal velocity is the superposition of the wave velocity and the current velocity:

$$u = \frac{\pi H}{T} \frac{\cosh k(z+d)}{\sinh kd} \cos(kx - \omega t + \varphi) + u_{\mathrm{current}} \tag{6}$$

where u is the horizontal velocity of fluid, u_{current} is the horizontal velocity of current, z is the vertical coordinate, d is the water deep.

The vertical velocity can be expressed as follows:

$$w = \frac{\pi H}{T} \frac{\sinh k(z+d)}{\sinh kd} \sin(kx - \omega t + \varphi) \tag{7}$$

where w is the vertical velocity of fluid.

2.4 Numerical Wave Absorption

A sponge layer wave absorption zone is set in the region near the outlet boundary to prevent wave reflection and absorb the current, i.e., a source term f_s is added within the wave absorption zone to achieve the wave absorption effect.

$$f_s(x) = -\rho\alpha_s \frac{(x - x_s)}{L_s}(U - U_{ref}) \tag{8}$$

where α_s is dimensionless viscosity coefficient, x_s is the starting position of the wave-breaking zone, L_s is the length of the wave-breaking zone, U_{ref} is the reference flow velocity.

2.5 Aerodynamic load calculation

This solver calculates the aerodynamic loads of the wind turbine based on the actuator line model. Its basic principle is to discretize the entire wind turbine blade into a number of blade element units. Each blade element unit is replaced by an actuator point to achieve the equivalent simulation of aerodynamic loads. The expression of the aerodynamic volume force is as follows:

$$f = (L, D) = \frac{1}{2}\rho U^2{}_{rel} c N_b (C_L e_L + C_D e_D) \tag{9}$$

where L and D are the lift and drag forces acting on the airfoil profile, U_{rel} is the relative wind speed at the blade cross-section, c is the chord length of the airfoil cross-section, N_b is the number of blades per wind turbine, C_L and C_D are the lift coefficient and drag coefficient respectively, e_L and e_D are the unit vectors in the x and y directions under the body-fitted coordinate system.

2.6 Mooring Model

The mooring model of this solver is independently developed based on the lumped mass method (LMM). As a type of finite difference method, the lumped mass method discretizes the continuous mooring chain into N nodes and N+1 segments, and performs force analysis on the nodes. The equilibrium equation is shown as follows:

$$M_{ti} a_i = T_i b_i - T_{i-1} b_{i-1} + \frac{1}{2}(B_{i-1}^{-1} f_{Di-1} + B_i^{-1} f_{Di}) - W_i \tag{10}$$

where M_{ti} is the sum of the node mass and the added mass, B_i is the transformation matrix for converting vectors from the global coordinate system to the local coordinate system, f_{Di} is the fluid resistance, a_i is the acceleration vector of node i, W_i is the gravity acting on the node i, T_i is the tension vector.

3. Calculation Model

In this work, the TLP platform equipped with the NREL 5MW wind turbine [8] is taken as the research object, and CFD numerical simulation studies on pure wave conditions and wave-current coupling conditions are carried out.

3.1 TLP Floating Wind Turbine Model

The TLP floating wind turbine is mainly composed of three parts: the wind turbine, the platform, and the mooring system.

The parameters of the NREL 5MW wind turbine are shown in the table 1 below:

TABLE 1: THE PARAMETERS OF THE NREL 5MW WIND TURBINE

Component	Parameter
Rotor Orientation, Configuration	Upwind, 3 Blades
Rotor, Hub Diameter	126 m, 3 m
Hub Height	90 m
Cut-In, Rated, Cut-Out Wind Speed	3 m/s, 11.4 m/s, 25 m/s
Cut-In, Rated Rotor Speed	6.9 rpm, 12.1 rpm
Rated Tip Speed	80 m/s
Overhang, Shaft Tilt, Precone	5 m, 5º, 2.5º
Rotor Mass	110,000 kg
Nacelle Mass	240,000 kg
Tower Mass	347,460 kg
Coordinate of Overall CM	(-0.2 m, 0.0 m, 64.0 m)

The parameters of the TLP and mooring system are shown in the table 2 below:

TABLE 2: NREL TLP AND MOORING SYSTEM PARAMETERS

Component	Unit	Parameter
Platform Mass	t	8600.41
Displacement	m^3	12179.6
Vertical center of gravity of the platform	m	-40.612
Draft	m	47.89
Water deep	m	200
Water density	kg/m^3	1025
Number of tendons	-	8
Nominal tendon pretension	kN	3931
Tendon diameter	m	0.127
Tendon mass per unit length	kg/m	116
Tendon axial stiffness modulus	N	1.5e9

3.2 Calculation Conditions

This work focuses on the differences in the motion responses of the TLP platform under pure wave conditions and wave-current coupling conditions. Therefore, the following two sets of operating conditions are selected for comparison. All wind conditions are steady winds, and all waves are regular waves. Since this study aimed to amplify the influence of ocean currents, relatively large current velocities and small wave heights were selected for the wave height and current parameters.

TABLE 3: WORKING CONDITIONS

	Wind (m/s)	Current (m/s)	Wave Period (s)	Wave Height (m)
Case 1	11.4	1.5	8.52	1.1
Case 2	11.4	0.0	8.52	1.1

3.3 Computation Domain Setting

The computational domain for the integrated analysis of the floating wind turbine is designed to be 1500 m in length, 400 m in width and 480 m in height. The distance between the TLP platform and the inlet boundary is 500 m; the height from the platform bottom to the free surface is 152.11 m; the distance from the platform to the left and right boundaries is 191 m respectively; and the length of the wave absorption zone is 200 m, as shown in Figure 1. The inlet boundary is set as the wave generation boundary condition; the outlet boundary is set as the zeroGradient; both the top and bottom boundaries are set as the slip; the front and back boundaries are set as the symmetric boundary; and the TLP is set as the wall.

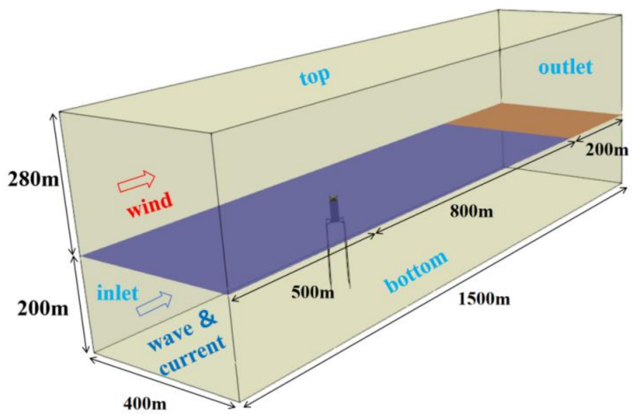

FIGURE 1: SIMULATION DOMAIN

3.4 Schematic Diagram of Mesh Generation

Based on Case 2, a mesh convergence analysis was performed with the surge RAO as the indicator of concern. Three sets of meshes with element counts ranging from coarse to fine were designed, and the surge RAOs were statistically evaluated. The results are presented in Table 4.

TABLE 4: MESH CONVERGENCE ANALYSIS

	Cell Number (Million)	Time step (s)	Surge RAO (m)
Coarse	3.41	0.02	0.232
Middle	7.97	0.01	0.211
Fine	12.89	0.005	0.210

After the mesh convergence analysis, a mesh scheme that balances computational accuracy and computational efficiency was finally selected, with a total number of approximately 7.97 million elements. Mesh refinement of Level 2 was performed near the free surface and the near-wake region respectively, while mesh refinement of Level 3 and Level 4 was carried out around the TLP platform based on the distance from the platform. Details of the mesh generation are shown in Figure 2.

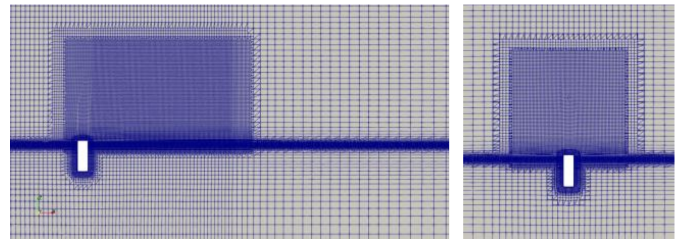

(a) *XOZ* plane (b) *YOZ* plane

FIGURE 2: SCHEMATIC DIAGRAM OF MESH GENERATION

3.5 Numerical Validation

The solver has been proven to have high accuracy in solving various platform motions and wind turbine wake flows [9]. No repeated validation is performed here, and reference can be made to the previous work.

4. RESULTS AND DISCUSSION

4.1 Motion Response Results

Given that the incident waves and ocean currents are aligned in the same direction and the TLP features a symmetric structural design, this study primarily focuses on three key degrees of freedom (DOFs) of the platform, namely surge, heave, and pitch motions. The time-history curves depicting the platform's dynamic responses under the two distinct operating conditions (i.e., with and without ocean current action) are presented in Figure 3 below. To facilitate in-depth analysis and comprehensive discussion of the platform's dynamic characteristics, the collected time-history curves were subjected to Fourier transform. Subsequently, statistical analysis was performed on the peak amplitude results corresponding to several specific frequencies extracted from the frequency-domain data, and the summarized findings are tabulated in Table 5 below.

The Fourier transform of the surge motion of the tension leg platform (TLP) reveals three dominant frequency peaks, corresponding to the slow drift, first-order wave-frequency motion and heave natural frequency respectively. Among these, the slow drift and first-order wave-frequency motion are the primary components, while the heave natura frequency arises from the coupling of the six degrees of freedom (DOFs) of the platform motion. As shown in Figure 3(a), the presence of ocean currents leads to a significant enhancement in the slow drift motion of the tension leg platform (TLP). Compared with the working condition without ocean currents, the mean value of the slow drift displacement increases by approximately 114%. In contrast, the influence of ocean currents on the wave-frequency motion component of the platform is relatively weak, which indicates that the wave-induced motion remains essentially unchanged under the effect of ocean current loads.

Fourier transform of the heave time-history results of the TLP shows that the heave motion is also excited by three frequencies, namely: slow drift, wave frequency and heave natural frequency. The difference from the surge motion is that the heave natural frequency dominates the heave motion. This unique characteristic of the TLP heave motion is directly attributable to the specific mooring characteristics of the tension leg platform. This is because the tension legs can provide a restoring force with extremely high stiffness, which exerts a significant influence on the natural heave frequency of the platform. As clearly illustrated in Figure 3(b), ocean currents induce a noticeable subsidence of the tension leg platform (TLP), shifting its static equilibrium position from +0.101 m to -0.284 m. This observable subsidence phenomenon can be attributed to the formation of a high-velocity and low-pressure zone at the bottom of the platform under the action of ocean currents. The high flow velocity at the platform bottom leads to a reduction in dynamic pressure, generating a downward suction force that drives the platform to sink. Meanwhile, ocean currents also exert an amplifying effect on the wave-frequency component of the heave motion, increasing its amplitude by approximately 133%. Nevertheless, the influence of ocean currents on the motion component corresponding to the platform's heave natural period is relatively limited, which indicates that the inherent heave dynamic characteristics of the platform are weakly affected by ocean current loads.

In addition, the results of the spectral analysis of the pitch motion exhibit high complexity, characterized by multiple significant frequency components and intricate interactions. Since the core focus of this study is to investigate the influence of wave-current coupling effects on the dynamic performance of the platform, no further in-depth discussion will be conducted herein on other frequency components appearing in the pitch motion. As shown in Figure 3(c), ocean currents alter the equilibrium position of the pitch motion of the tension leg platform (TLP). This change in the pitch equilibrium state is mainly attributed to the fact that the hydrodynamic torque exerted by ocean currents on the platform is opposite in direction to the aerodynamic torque generated by wind loads. The opposing torques partially counteract each other, thereby shifting the platform's pitch equilibrium state. In addition, quantitative results indicate that ocean currents slightly reduce the amplitude of the wave-frequency component of the platform's pitch motion by approximately 8%. Nevertheless, since the amplitude of the TLP's inherent pitch motion is extremely small under the studied operating conditions, the overall impact of ocean currents on the platform's pitch performance is deemed negligible.

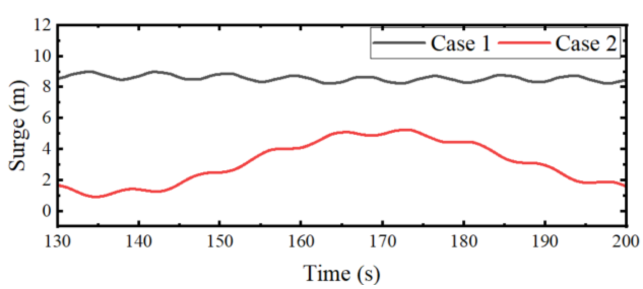

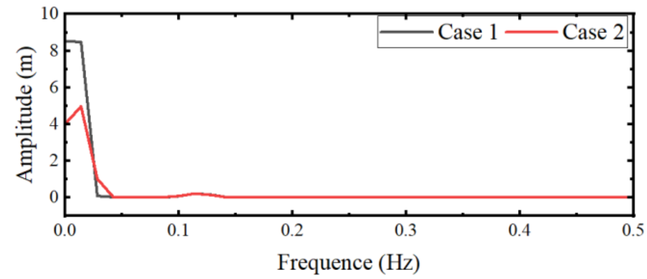

(a) Surge

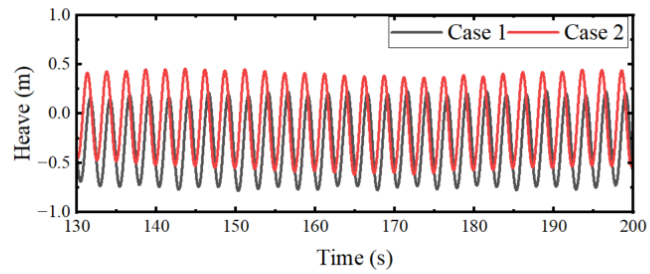

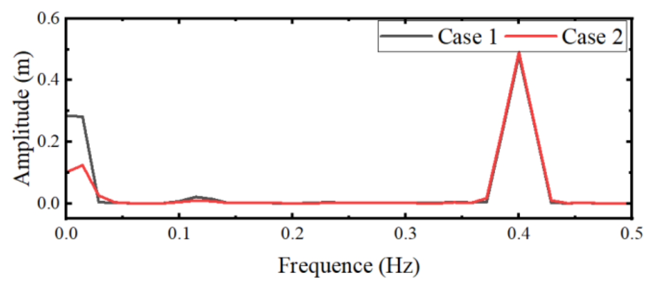

(b) Heave

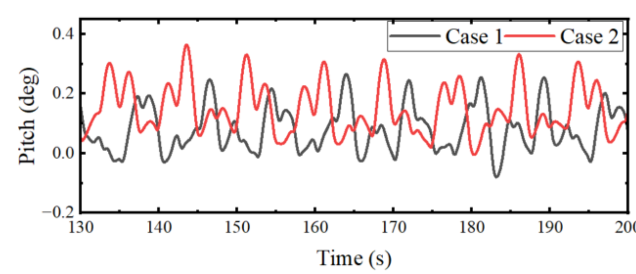

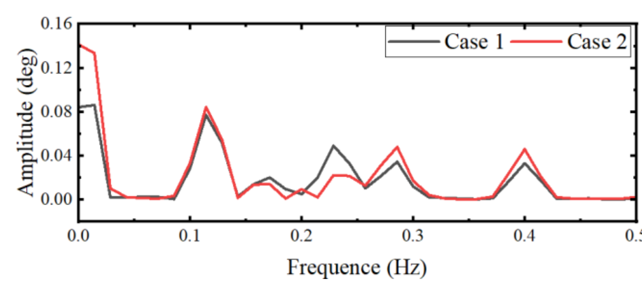

(c) Pitch

FIGURE 3: TIME-HISTORY CURVE AND FFT RESULT OF MOTION

TABLE 5: MOTION STATISTICAL RESULTS

		Mean (m)	Wave Frequence (m)	Heave Natural Frequence (m)
Surge	Case 1	8.542	0.217	0.016
	Case 2	3.993	0.211	0.006
Heave	Case 1	0.284	0.021	0.480
	Case 2	0.101	0.009	0.490
Pitch	Case 1	0.084	0.077	0.033
	Case 2	0.142	0.084	0.046

Figure 4 presents the directional components of the mooring force for the TLP platform under two operating conditions. It can be observed that the current load leads to a significant increase in the peak value of the horizontal mooring force. According to the spectral analysis results, the effect of the current load on the platform is not only reflected in the shift of the equilibrium position, but also results in a distinct increase in the high-frequency components of the mooring load. For instance, in the spectral analysis of the X-direction component of the mooring force, the peak values at frequencies of 0.4 Hz and 0.8 Hz both increase noticeably.

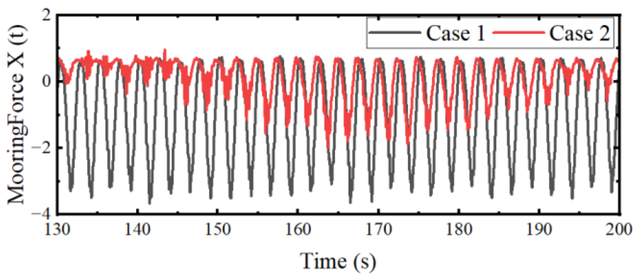

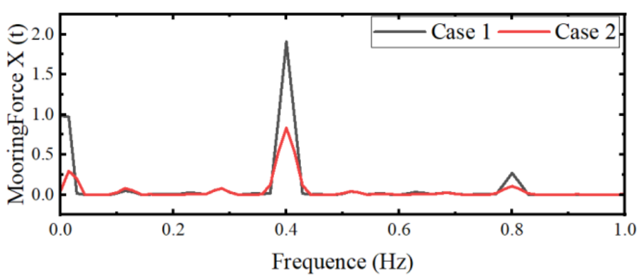

(a) Horizontal X-component of mooring force

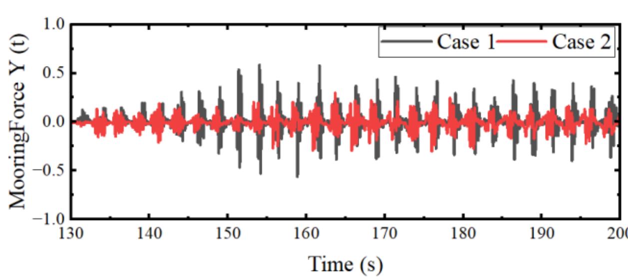

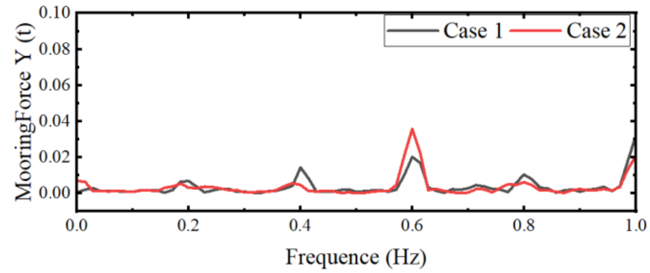

(b) Horizontal Y-component of mooring force

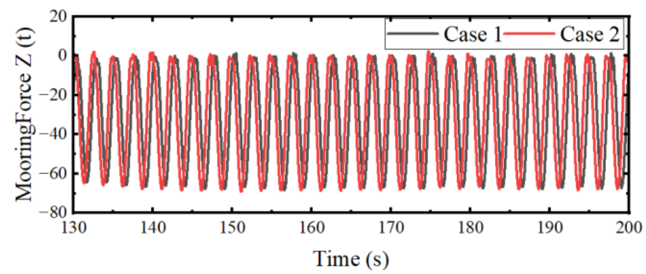

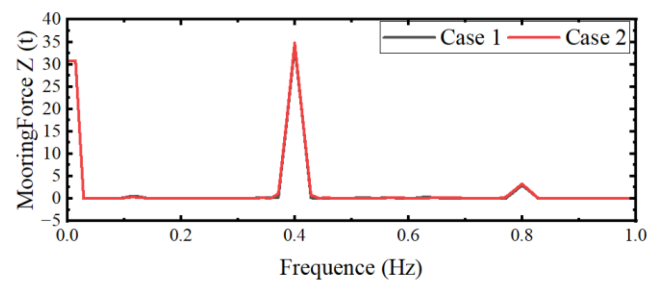

(c) Vertical Z-component of mooring force

FIGURE 4: TIME-HISTORY CURVE AND FFT RESULT OF MOORING FORCE

4.2 Detailed Analysis of Flow Field

As can be seen from Figure 5, when the Tension Leg Platform (TLP) is subjected solely to wind and wave loads without the superposition of ocean current loads, the vertical heave motion of the platform will induce a periodic oscillating flow field with a concentric-circle-like pattern at the free surface of the surrounding water body. This concentric-circle-like flow field propagates radially outward in all directions, with its intensity gradually decaying. During the diffusion process, it interacts with the surrounding fluid, continuously dissipating energy until it is completely dissipated and merges with the surrounding static water body. In stark contrast, when ocean currents act on the TLP, the platform is subjected to a continuous horizontal thrust generated by the currents, which pushes it away from its initial equilibrium position and causes a slight yet stable offset along the current direction. Meanwhile, due to the blocking effect of the TLP structure on the incoming currents, a distinct wake zone with obvious velocity deficit is formed in the downstream area along the current direction. The flow within this wake zone is highly turbulent, the velocity magnitude is significantly lower than that of the incoming currents, and complex vortex structures are continuously generated and shed.

In addition, it can be clearly observed from the detailed dynamic pressure distribution results around the TLP that under the combined influence of ocean currents and the platform's offset motion, a distinct low-pressure zone appears in the wake area behind the TLP. This low-pressure zone is closely related to the velocity deficit in the wake zone; the pressure values in this zone are significantly lower than those in the upstream area of the platform and the surrounding flow field, which in turn exerts an impact on the overall hydrodynamic loads acting on the TLP.

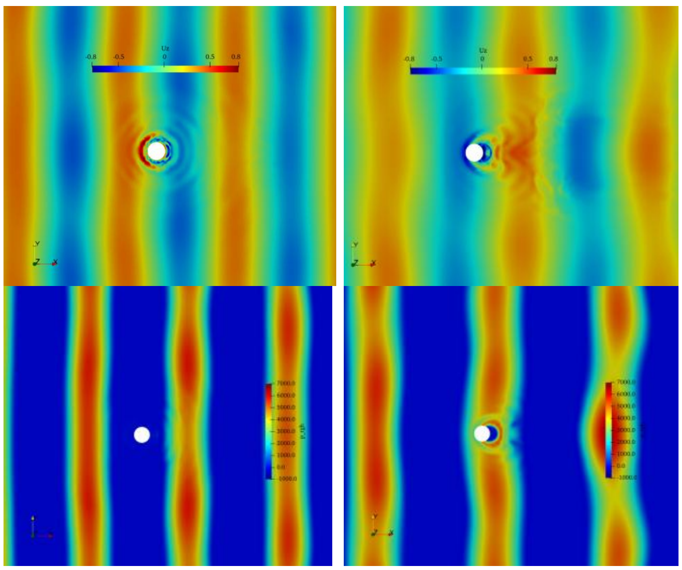

(a) Case 1 (b) Case 2

FIGURE 5: RESULTS OF FREE SURFACE FLOW FIELD

As can be seen from Figure 6, when the Tension Leg Platform (TLP) is subjected only to wind and wave loads without the superposition of ocean current loads, the horizontal flow velocity distribution of the water around the platform presents an almost perfectly symmetrical pattern in the lateral direction. Meanwhile, under the oscillating flow field induced by the interaction between the platform structure and waves, the water at the TLP edges continuously separates and reattaches due to viscosity, thus forming several local vortex structures with relatively regular shapes. However, under the combined action of wind, wave and current loads, the originally symmetrical horizontal flow velocity distribution around the TLP is completely disrupted. A low-velocity zone with an obvious velocity gradient is formed in the downstream area of the platform along the current direction; this low-velocity zone gradually extends upward from the platform bottom to the free surface, thereby interfering with the velocity magnitude and direction of the surrounding water over a wide range.

In contrast, the flow velocity at the bottom of the TLP remains relatively high, which is mainly attributed to the blocking effect of the platform structure on the incoming flow and the intensified flow mixing effect induced by the vortex structures. In addition, it can be seen from the detailed dynamic pressure distribution data at the TLP bottom that compared with the case without ocean currents, the dynamic pressure at the platform bottom decreases significantly when ocean currents are present.

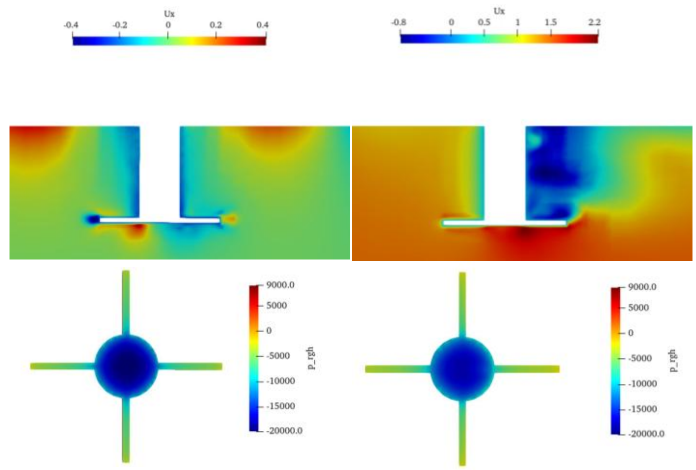

(a) Case 1 (b) Case 2

FIGURE 6: RESULT OF THE FLOW FIELD AROUND TLP

As can be seen from the results of Figures 7 and 8, although ocean currents affect the motion of the TLP, their influence on the wind turbine wake is negligible. There are almost no significant differences in the key wake characteristics between the cases with and without ocean currents. Specifically, Figure 6 shows that the spatial diffusion range and flow field distribution characteristics of the wind turbine wake are basically consistent under the two working conditions. Similarly, Figure 7 shows that no obvious changes are observed in the wake structure and velocity amplitude distribution between the scenarios with and without ocean currents. This indicates that under the research conditions of this study, the presence of ocean currents does not alter the inherent evolution law of the wind turbine wake, and thus the impact of ocean currents can be ignored when analyzing the wake characteristics of the wind turbine mounted on the TLP platform.

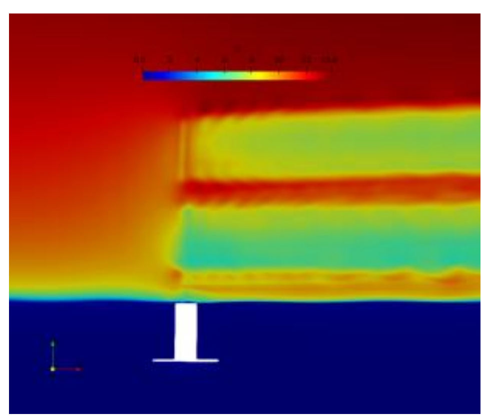

(a) Case 1

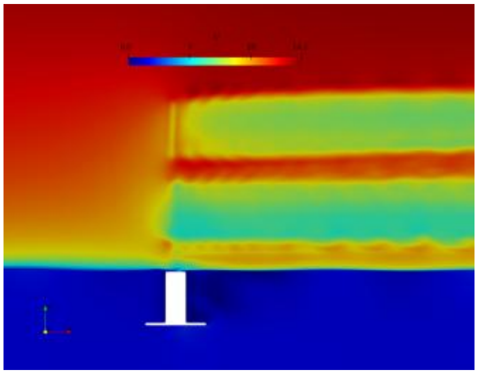

(b) Case 2

FIGURE 7: *XOZ* PLANE VIEW OF WIND TURBINE WAKE

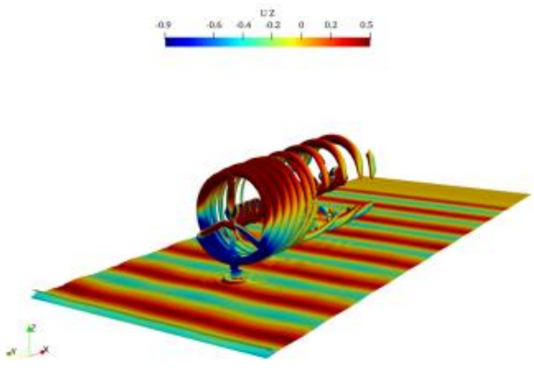

(a) Case 1

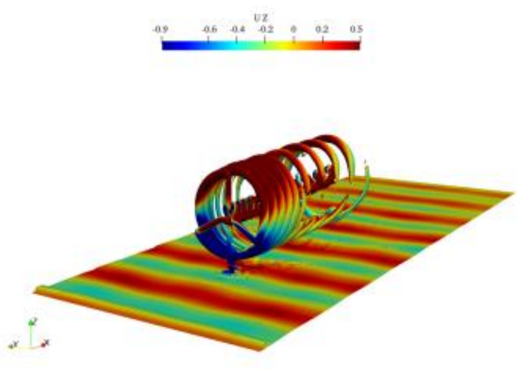

(b) Case 2

FIGURE 8: ISO-SURFACE OF Q = 0.01, COLORED BY VELOCITY

5. CONCLUSION

Based on the in-house solver FOWT-ULAM-SJTU, this work conducts numerical simulations of wind-wave and wind-wave-current coupling for the TLP platform equipped with the NREL 5MW wind turbine. It compares and analyzes the time-domain motion curves and frequency-domain component results, explains the causes of differences based on the flow field characteristics, and finally draws the following conclusions:

(1) Ocean currents exert differential impacts on the TLP's three key DOFs: they boost surge slow drift by 114%, induce heave subsidence and amplify its wave-frequency amplitude by 133%, and marginally affect pitch with negligible overall influence.

(2) Ocean currents significantly reshape the TLP-surrounding flow field: without currents, TLP heave creates a dissipating concentric free-surface flow; with currents, the TLP shifts, forming wake/low-pressure zones and disrupting velocity symmetry.

ACKNOWLEDGEMENTS

This work was supported by the National Key Research and Development Program of China (2025YFF0515700), to which the authors are most grateful.

REFERENCE

[1] J.R.O. Marsh, Marine Platforms: US (1959).

[2] Y. Huang, P. Cheng, D.C. Wan, Numerical Analysis of a Floating Offshore Wind Turbine by Coupled Aero-Hydrodynamic Simulation, Jounal of Marine Science and Engineering 18 (2019) 82–92.

[3] Y.J. Ren, W. Shi, V. Venugopal, et al, Experimental study of tendon failure analysis for a TLP floating offshore wind turbine, Applied Energy 358 (2024) 122633.

[4] J.M. Jonkman, M.L. Buhl, FAST User's Guide. NREL, 2005.

[5] J.R. Paulling, E.E. Horton, Analysis of the Tension Leg Platform, Society of Petroleum Engineers Journal 11 (1971) 285-294.

[6] P. Cheng, Y. Huang, D.C. Wan, A numerical model for fully coupled aero-hydrodynamic analysis of floating offshore wind turbine, Ocean Engineering 173 (2019) 183-196.

[7] J.N. Sorensen, W.Z. Shen, Numerical Modeling of Wind Turbine Wakes, Journal of Fluids Engineering 124 (2002) 393-399.

[8] J.M. Jonkman, S.M. Butterfield, W. Musial, et al, Definition of a 5-MW reference wind turbine for offshore system development, Golden, USA: National Renewable Energy Lab (2009).

[9] Y. Huang, W. Zhao, D.C. Wan, Numerical simulation of coupled aero-hydro-elastic performance of floating offshore wind turbine, Ocean Engineering 40 (2022) 88-101.